Kawasaki, A; Inakawa, T; Kasahara, J; Goto, K; Matsuoka, K; Matsuo, A; Funaki, I, Critical condition of inner cylinder radius for sustaining rotating detonation waves in rotating detonation engine thruster, PROCEEDINGS OF THE COMBUSTION INSTITUTE, 37, 3, 2019, 3461-3469

Title:	**Critical Condition of Inner Cylinder Radius for Sustaining Rotating Detonation Waves in Rotating Detonation Engine Thruster**
Authors:	AKIRA KAWASAKI[1], TOMOYA INAKAWA[1], JIRO KASAHARA[1], KEISUKE GOTO[1], KEN MATSUOKA[1], AKIKO MATSUO[2], IKKOH FUNAKI[3]
Affiliation 1:	Department of Aerospace Engineering, Nagoya University Furo-cho, Chikusa-ku, Nagoya, Aichi 464-8603, Japan
Affiliation 2:	Department of Mechanical Engineering, Keio University 3-14-1 Hiyoshi, Kouhoku-ku, Yokohama, Kanagawa 223-8522, Japan
Affiliation 3:	Institute of Space and Astronautical Science, Japan Aerospace Exploration Agency 3-1-1 Yoshinodai, Chuo-ku, Sagamihara, Kanagawa 252-5210, Japan
Corresponding author's contact information	JIRO KASAHARA, Department of Aerospace Engineering, Nagoya University Furo-cho, Chikusa-ku, Nagoya, Aichi 464-8603, Japan E-mail: kasahara@nuae.nagoya-u.ac.jp Fax: +81-52-789-4404
Colloquium:	DETONATIONS, EXPLOSIONS, AND SUPERSONIC COMBUSTION
Total Length:	6189 words (Method 1)

Main text:	3135 words
Equations:	15 words
Nomenclature:	212 words
References:	524 words
Table 1:	243 words
Figure 1:	352 words
Figure 2:	528 words
Figure 3:	541 words
Figure 4:	242 words
Figure 5:	132 words
Figure 6:	132 words
Figure 7:	132 words

Table

Table 1 Experimental conditions and summary of results

List of figure captions

Abstract

We describe the critical condition necessary for the inner cylinder radius of a rotating detonation engine (RDE) used for in-space rocket propulsion to sustain adequate thruster performance. Using gaseous C_2H_4 and O_2 as the propellant, we measured thrust and impulse of the RDE experimentally, varying in the inner cylinder radius r_i from 31 mm (typical annular configuration) to 0 (no-inner-cylinder configuration), while keeping the outer cylinder radius (r_o = 39 mm) and propellant injector position (r_{inj} = 35 mm) constant. In the experiments, we also performed high-speed imaging of self-luminescence in the combustion chamber and engine plume. In the case of relatively large inner cylinder radii (r_i = 23 and 31 mm), rotating detonation waves in the combustion chamber attached to the inner cylinder surface, whereas for relatively small inner cylinder radii (r_i = 0, 9, and 15 mm), rotating detonation waves were observed to detach from the inner cylinder surface. In these small inner radii cases, strong chemical luminescence was observed in the plume, probably due to the existence of soot. On the other hand, for cases where r_i = 15, 23, and 31 mm, the specific impulses were greater than 80 % of the ideal value at correct expansion. Meanwhile, for cases r_i = 0 and 9 mm, the specific impulses were below 80 % of the ideal expansion value. This was considered to be due to the imperfect detonation combustion (deflagration combustion) observed in small inner cylinder radius cases. Our results suggest that in our experimental conditions, r_i = 15 mm was close to the critical condition for sustaining rotating detonation in a suitable state for efficient thrust generation. This condition of the in the inner cylinder radius corresponds to critical condition to the condition in the reduced unburned layer height of

4.5–6.5.

Keywords

Rotating detonation engine, critical condition of detonation, detonation

Nomenclature

A_c = cross-sectional area of combustion chamber, $\pi (r_o^2 - r_i^2)$

A_{inj} = total area of injection halls

A_o = cross-sectional area of outer cylinder, πr_o^2

C_c = calibration constant for mass flow rate

D = detonation velocity

f_{DW} = detonation frequency

g_0 = gravitational acceleration at sea level

h = height of injected unburnt mixture layer

I_{sp} = specific impulse (evaluated based on thrust and mass flow rate)

$\dot{m}$ = propellant mass flow rate

n_{DW} = number of detonation wave

p_b = backpressure

p_c = pressure of combustion chamber

p_{ple} = pressure of plenum chamber

R = gas constant

r_i = inner cylinder radius of combustion chamber

r_{inj} = radial position of the centerline of propellant injection halls

r_o = outer cylinder radius of combustion chamber

T = temperature

γ = specific heat ratio

λ = detonation cell width

ρ = density

ϕ = propellant equivalence ratio of

1. Introduction

Detonation, which is one form of combustion wave traveling in a premixed fuel-oxidizer mixture in the gas phase, has remarkable characteristics in that it can attain higher combustion temperature and speed than deflagration, the other form of combustion wave, given the same initial conditions [1–3]. Because higher combustion temperature

can lead to higher thermal efficiencies in a thermodynamic cycle, and higher combustion speed can lead to completion of combustion at shorter distances, many researchers are attempting to utilize detonation in combustion engines, including propulsion devices (e.g., rocket and jet engines).

Propulsion devices utilizing detonation can generally be classified into two types: the pulse detonation engine (PDE), and the rotating detonation engine (RDE) [4]. A PDE generates thrust by intermittent detonation combustion in a tube-shaped combustor, and has a remarkable advantage in terms of controllability of the total impulse compared to RDE [5]. On the other hand, an RDE generates thrust by continuous detonation combustion, which is maintained in its combustion chamber in the form of a rotating detonation wave [6–8]. RDE can usually exert higher thrust densities than PDE, because with continuous combustion, the throughput of the propellant can also be high. Hence RDEs are currently attracting increased attention as primary thrusters for space and aircraft propulsion.

Typically, the combustion chamber of an RDE is a narrow, annular channel, and thus consists of inner and outer cylinders. Several studies characterized the structure of rotating detonation waves in RDE combustors with annular combustion chambers. Nakayama et al. [9–10], Kudo et al. [11], and Sugiyama et al. [12] investigated the structure of detonation waves propagating within curved channels filled with fuel-oxidizer mixtures, and discussed the critical condition in channel curvature for the stable propagation of a rotating detonation wave. On the other hand, there are some variants in the combustion chamber geometry of RDE. Bykovskii et al. [6, 13] realized stable rotating detonation waves in disk-shaped combustion chambers. They visualized the detonation waves in the combustion

chambers by a streak camera, and proposed the basic flow structure. Nakagami et al. [14–15] further investigated the structure of rotating detonation waves in a disk-shaped combustion chamber. Tang, Wang, and Shao [16] proposed another geometry for the combustion chamber, i.e., a cylindrical chamber similar to the annular one but without an inner cylinder. Using this cylindrical combustion chamber, they performed 3-D flow simulation with a single-step chemical kinetics model, and concluded that detonation waves could rotate continuously in the chamber. In experiments, Wei et al. [17] and Anand et al. [18] later confirmed stable realization of rotating detonation waves in an RDE with a cylindrical combustion chamber although thrust was not measured in their studies.

Here, a cylindrical RDE with no inner cylinder can lead to realization of a smaller and simpler RDE compared to typical annular RDEs, because removing the inner cylinder makes it possible to reduce not only the size of the combustion chamber for an identical cross-sectional area, but also the cooling arrangement for the inner cylinder. Therefore, the cylindrical RDE may be a preferable option, and could be particularly important for in-space propulsion devices. However, the impact of removing the inner cylinder from the RDE has not yet been fully clarified. In the present study, we measure thrust in an RDE using gaseous ethylene and oxygen as the propellant, and varying the inner-cylinder radius r_i from 31 mm (typical annular configuration) to 0 (no-inner-cylinder configuration) under a constant outer cylinder radius r_o = 39 mm and propellant injection position r_{inj} = 35 mm. We perform high-speed imaging of self-luminescence in the combustion chamber and engine plume to identify the characteristics of the combustion.

2. Experimental Setup

Figure 1 presents a cross-sectional schematic of the RDE investigated in this study. The RDE had separate fuel and oxidizer plenum chambers, and a doublet impinging-type propellant injector plate at the bottom of the combustion chamber. In Fig. 1, a cylindrical coordinate system is defined as the z-direction corresponds to the symmetry axis. The origin of the coordinate system is at the intersection of the symmetry axis and injector surface. The outer cylinder wall of the combustion chamber is at r_o = 39 mm, and its outlet is at z_h = 70 mm. The radial location of the inner cylinder wall of the combustion chamber, the inner cylinder radius r_i, was varied in a range from 0–31 mm. The diameter of both the fuel and oxidizer injection holes was 1 mm. There were 120 injection holes in each. The centerline of the injection holes was located at r_{inj} = 35 mm, and the radial distance between the centers of neighboring fuel and oxidizer injection holes, constituting a doublet, was 3.0 mm.

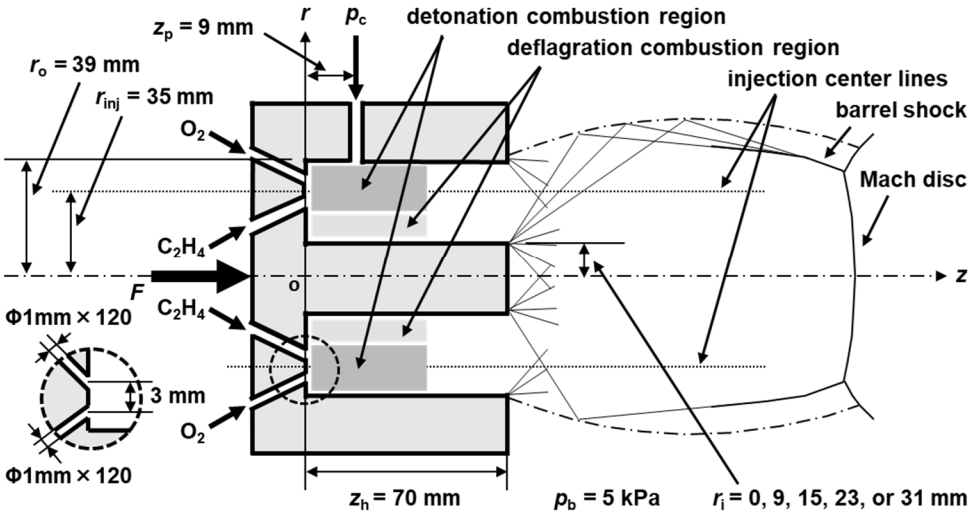

Fig. 1. Cross-section schematic of RDE.

An experiment was conducted using a vacuum combustion facility that consisted mainly of a vacuum chamber, thrust stand, and propellant supply system. The vacuum chamber had a volume of 30.1 m^3, and could be evacuated by two rotary pumps. The RDE was attached to a sliding platform on the thrust stand. This platform had one horizontal translational degree of freedom, was rigidly fixed to the main body of the thrust stand through a load cell (MODEL-DUD/Aikoh Engineering). The load cell measured the thrust.

The propellant supply system consisted mainly of fuel and oxidizer tanks, pneumatic valves, and orifices. The gaseous ethylene and oxygen used as the propellant were supplied to the plenum chambers of the RDE. Mass flow rates of fuel and oxidizer were regulated by changing the diameter of the orifices along the supply lines. Flows in the supply lines were choked at the orifices and injection holes before ignition by keeping the pressure of tanks and plenum chambers, and the pressure ratios across orifices and injection holes sufficiently high [19]. Although the pressure ratio across injection holes could sometimes be less than the critical pressure ratio after ignition, due to the rise in combustion-chamber pressure, the mass flow rate in the supply line was kept constant because the choking condition was satisfied at the orifice. In the experiments, mass flow rates were evaluated based on the total cross-section area of the injection holes and plenum pressures before ignition with Eq. (1) [20].

$$\dot{m} = C_c p_{\mathrm{ple}} A_{\mathrm{inj}} \sqrt{\frac{\gamma}{RT_0}\left(\frac{2}{\gamma+1}\right)^{(\gamma+1)/(\gamma-1)}} \tag{1}$$

The calibration constant C_c in Eq. (1) was preliminarily determined by comparing a known mass flow rate with the

right-hand side of Eq. (1). The error of the mass flow rate was mainly attributed to error in the calibration constant, and this error was evaluated to be less than 10 %.

The experimental procedure was as follows. The vacuum chamber was first evacuated to a designated pressure p_b. The propellant was then supplied to the RDE. Once the propellant had attained a steady state, an initiator, or pre-detonator, ignited the RDE in response to an ignition signal. After 0.4-s operation, the valves were closed, and the combustion was terminated. Because the capacities of the propellant tanks are sufficiently large, the mass flow rates were kept approximately constant during RDE operation, i.e., the decreases in the mass flow rate were less than 3 %. During operation, the time histories of thrust F, combustion-chamber pressures p_c, fuel and oxidizer plenum chambers p_{ple}, and backpressure p_b were recorded by a data logger. Combustion chamber pressure p_c was measured via a pressure port in the outer cylinder 9-mm downstream from the injector surface. High-speed cameras were also employed to record sequential images of self-luminescence in the combustion chamber and engine plume.

3. Results and Discussion

The experimental conditions and a summary of the measurement results are listed in Table 1. The inner cylinder radius r_i was varied at 0, 9, 15, 23, and 31 mm. Note that an inner cylinder radius of 0 mm essentially means a no-inner-cylinder configuration. Throughout the all RDE runs, the propellant mass flow rate $\dot{m}$ and equivalence ratio ϕ were controlled within the range of 136±6 g/s and 1.18±0.17, respectively (aside from measurement errors). The backpressure p_b, or vacuum chamber pressure, was in the range of 5±1 kPa before each operation. Combustion

chamber pressure p_c, and thrust F, were evaluated as time-averaged values. The specific impulse I_{sp} was evaluated with $I_{sp} = F/\dot{m}g_0$. The number of detonation wave n_{DW}, detonation frequency f_{DW}, and detonation velocity D were evaluated based on the observation by high-speed cameras. For all inner-cylinder radii, including the no-inner-cylinder configuration (r_i = 0 mm), the RDE operated with rotating detonation waves.

Table 1. Experimental conditions and summary of results

Run #	r_i [mm]	$\dot{m}$ [g/s]	ϕ [-]	p_c [kPa]	F [N]	I_{sp} [s]	n_{DW} [-]	f_{DW} [kHz]	D [m/s]
1	0	130±13	1.19±0.1	47±3	200±10	156±16	1	10.8±0.3	2370±50
2	9	138±14	1.13±0.1	47±3	237±12	175±17	1	10.5±0.3	2300±50
3	15	132±13	1.01±0.1	48±3	251±13	194±19	1	8.6±0.3	1900±50
4	23	133±13	1.01±0.1	61±3	265±13	203±20	1	10.8±0.3	2380±50
5	31	135±14	1.01±0.1	120±3	303±15	229±23	2	18.9±0.3	2080±50
6	0	131±13	1.12±0.1	47±3	221±11	173±17	1	10.7±0.3	2360±50
7	0	135±14	1.34±0.1	51±3	225±13	171±17	1	10.6±0.3	2340±50
8	0	136±14	1.18±0.1	47±3	225±13	168±17	1	10.1±0.3	2210±50
9	31	135±14	1.28±0.1	123±3	312±15	236±24	2	19.0±0.3	2090±50
10	31	136±14	1.09±0.1	140±3	306±15	229±23	3	24.3±0.3	1780±50
11	31	140±14	1.10±0.1	140±3	303±15	222±22	3	24.3±0.3	1780±50
12	31	142±14	1.09±0.1	126±3	306±15	220±22	2	18.9±0.3	2080±50

3.1. Structure of Flow and Combustion Field

To summarize this section, Fig. 1 proposes a schematic illustration of the flow and combustion fields of an RDE deduced from axial and lateral direction images of the self-luminescence. The axial-direction images of the inside of the combustion chamber showed regions where detonation or deflagration combustion occurred. Meanwhile lateral-

direction images of the exhaust plumes revealed Mach-disk-like discontinuity. In this study, non-detonation combustion was regard as deflagration combustion in accordance with accepted definitions (e.g. [3]). We identified the deflagration region based on the following: (1) strong illuminants generated in the combustor were observed in the lateral photographs of the plume (Fig. 3) for small inner cylinder cases, indicating incomplete detonation combustion within the combustor; and (2) as per previous studies, deflagration regions are supposed to arise adjacent to detonation regions [21].

Figure 2 shows typical axial photographs of self-luminescence in the combustion chamber for run number 1–5. The interval between frames was 6.25 μs. In the case of r_i = 0 and 23 mm, images have been vertically reflected for ease of comparison with the other cases. In the case of r_i = 0, 9, 15, and 23 mm, single rotating detonation waves can be observed, whereas two rotating detonation waves are observed in the case of r_i = 31 mm. Additionally, detonation waves attach to the inner cylinder wall in the case of r_i = 23 and 31 mm, whereas they detached from the inner cylinder wall in the case of r_i = 0, 9, and 15 mm. In conjunction with this, the specific impulse deteriorated in the case of r_i = 0 and 9 mm as described below. Thus, we regard the case where r_i = 15 mm as the critical case to sustain the rotating detonation wave in a suitable state for efficient thrust generation. The cases with larger inner cylinder radius (r_i = 23 and 31 mm) and smaller inner cylinder radius (r_i = 23 and 31 mm) were classified into supercritical and subcritical cases, respectively.

As may be seen in Fig. 2, different regional characteristics were observed in all cases. These included relatively

sharply outlined regions, which can be interpreted as detonation waves, and relatively vaguely outlined regions with rather weak luminescence, which can be interpreted as the consequence of non-detonation combustion. The region with weak luminescence appeared to expand with a decrease of the inner cylinder radius. In a numerical simulation for an RDE with the no-inner-cylinder configuration [16], rotating detonation waves attached to the outer wall, while non-detonation (i.e., deflagration) combustion occurred in an inner region of the combustor. Our observations were in good accord with these characteristics of the combustion structure.

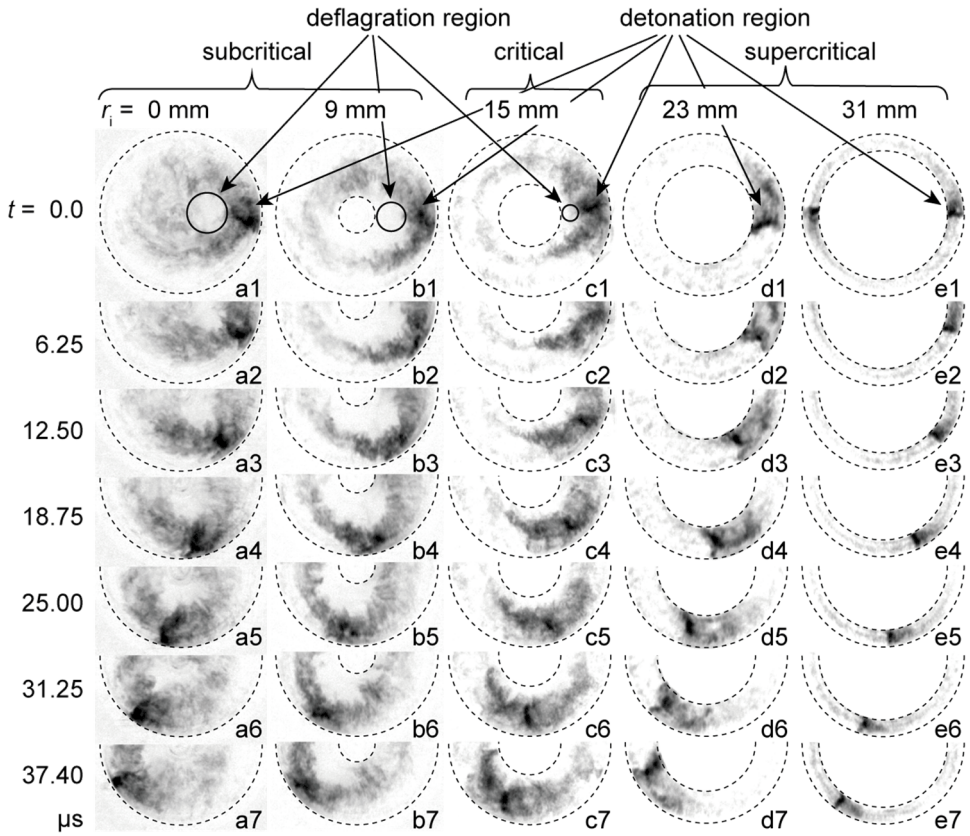

Fig. 2. Typical axial images of self-luminescence in the combustion chamber taken with a high-speed camera (C_2H_4–O_2, ϕ = 1.18±0.17, $\dot{m}$ = 136±6 g/s, p_b = 5±1 kPa). Black and white was inverted. For r_i = 0 and 23 mm, the images are reflected vertically. See also Supplemental Material, Movies S2(a), (b), (c), (d), and (e).

Figure 3 shows typical lateral images of the self-luminescence of exhaust plumes for run number 1–5. In all cases, Mach-disk-like discontinuities of luminescence can be observed, and these become sharper with an increase of the inner cylinder radius. As may be seen, for example, in Fig. 3(e3), some discontinuities connecting with the Mach-disk-like discontinuity are visible upstream of it. These should be interpreted as oblique shock waves, and their upstream edges do not seem to connect with the outer cylinder outlet edge of the combustion chamber. This is thought to mean that there are barrel shocks downstream of the outlet, and the exhaust plumes are supersonic and under expansion. In the case of $r_i = 0$, and 9 mm (subcritical cases), and 15 mm (critical case), there are areas where strong chemical luminescence of soot can be seen, as shown in Fig. 3. This is due to incomplete combustion in the deflagration combustion region, as shown in Fig. 1.

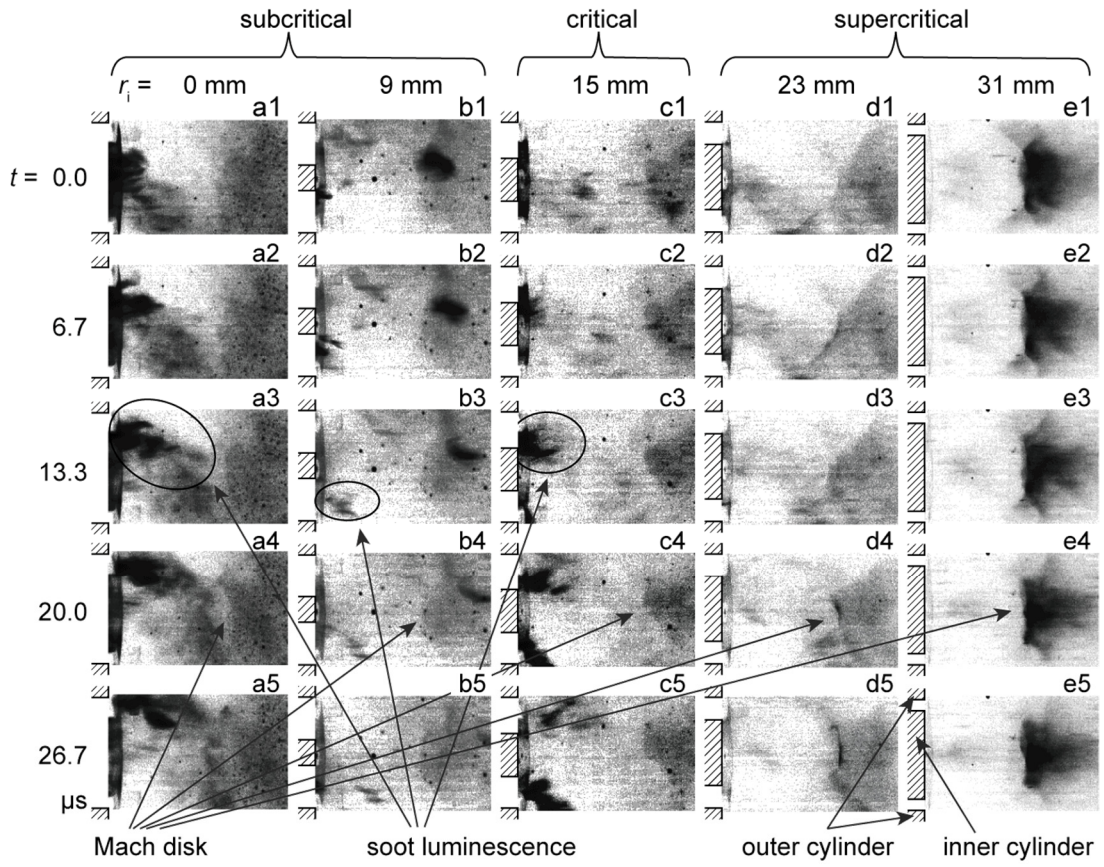

Fig. 3. Typical lateral images of self-luminescence of exhaust plume taken with a high-speed camera (C_2H_4–O_2, ϕ = 1.18±0.17, $\dot{m}$ = 136±6 g/s, p_b = 5±1 kPa). Black and white was inverted. See also Supplemental Material, Movies S3(a), (b), (c), (d), and (e).

3.2. Thrust and Impulse Performance

Figure 4 shows the time history of the thrust and pressure of combustion chamber. The origin of the time axis was set to that of the ignition signal. In Fig. 4(a), thrusts of approximately 50 N can be seen before ignition. This is due to cold gas jets without combustion. After ignition, thrusts rise and reach steady states by 0.2 s. In Fig. 4(b), plateaus can be seen also for pressure histories during combustion as with the case of thrust. To obtain time-averaged thrust F and pressure of the combustion chamber p_c, we used the region between the two dashed lines in Fig 4, i.e., t

= 0.2–0.35 s. In a stable operation, the averaged values of thrust and combustion chamber pressure are independent of the time region if the region is selected from the plateau of the time history. Thus, from the viewpoint of ease of data processing, we chose the same time region for all cases. The detonation frequencies *f* were also evaluated as time-averaged values. However, time history of the detonation frequency cannot be directly recorded by the data logger, but has to be reduced from sequential images recorded by the high-speed cameras. Thus, the detonation frequencies were evaluated as inverses of averaged rotating periods of detonation waves in arbitrary 10 revolutions within the time region stated above, i.e., t = 0.20.35 s, also for ease of data processing. In general, the detonation frequency is constant as long as the operation is stable (see, for e.g., [22]). We confirmed that difference in a 10-revolution-averaged value is equivalent to 20-revolution-averaged value within an error of 1 %, and the 10-revolustion-averaged value has a sufficient accuracy. The propagation speed of detonation waves D was calculated with $D = 2\pi r_{\mathrm{inj}} f_{\mathrm{DW}} / n_{\mathrm{DW}}$. Note that the circumferential length at the centerline radius of the injection holes r_{inj} = 35 mm was used for the calculation of the displacement of detonation waves.

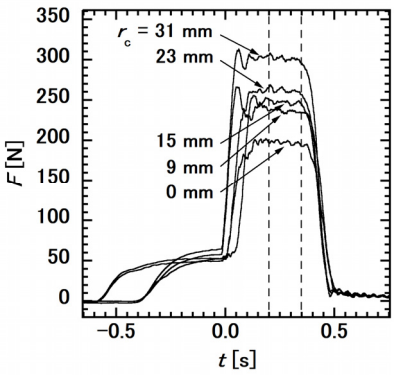

(a) Thrust

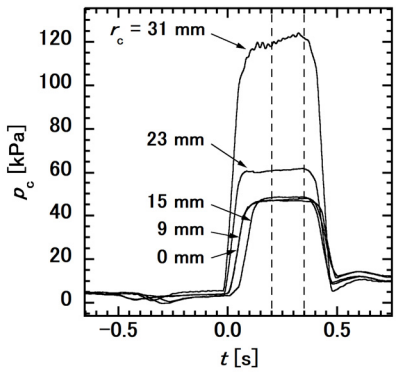

(b) Pressure of the combustor chamber

Fig. 4. Time histories of measured data (C_2H_4–O_2, ϕ = 1.18±0.17, $\dot{m}$ = 136±6 g/s, p_b = 5±1 kPa). Dashed lines indicate time region for averaging.

As shown in Table 1, the propagation speed of detonation waves was 2300 m/s except for the cases r_i = 15 and 31 mm (1760 m/s for the r_i = 31 mm), whereas the Chapman–Jouguet (C–J) detonation velocity is 2800 m/s for ethylene-oxygen mixture. The velocity deficit of detonation waves in an RDE, which can be as low as 40 % of C–J velocity [26], is thought to be due mainly to the curvature effect, incomplete mixing of fuel and oxidizer, and dilution of the fuel-oxidizer mixture by burned gas. This phenomenon has been confirmed both experimentally and numerically by many researchers (e.g., [6, 21]). In general, the velocity deficits in RDEs are enhanced with increases in the number of detonation wave heads in combustors (e.g., [6]). However, the impact of reduced wave speed on RDE performance is not significant [21]. It is also known that the number of detonation wave heads increases with the propellant mass flux in the combustor [6].

Figure 5 shows dependence of combustion chamber pressure p_c on cross-section area ratio A_c / A_o. As shown in the figure, the pressure decreases with the increase in channel cross-sectional area A_c; i.e., with the decrease in the

inner cylinder radius. The pressure trend is approximately inversely proportional to the channel cross-sectional area. This is because injected propellant undergoes more significant expansion in a wider chamber. As a result, the thrust did not decrease with the increase of the inner cylinder radius.

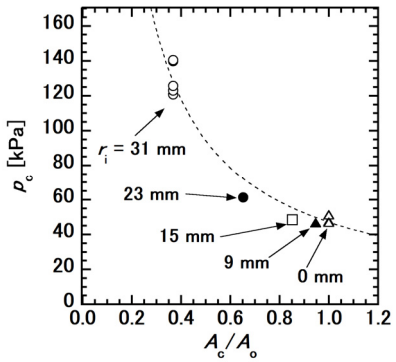

Fig. 5. Dependence of combustion chamber pressure on cross-section area ratio (C_2H_4–O_2, ϕ = 1.18±0.17, $\dot{m}$ = 136±6 g/s, p_b = 5±1 kPa). Dashed line is an inversely proportional curve.

Figure 6 plots the specific impulse I_{sp} versus the combustion pressure p_c. In Fig. 6, ideal specific impulse at correct expansion $I_{sp,correct}$ was also shown as a function of the pressure of the combustion chamber by a solid line. The ideal specific impulse was computed using the NASA-CEA code [23] for an equivalence ratio of 1.14 and a backpressure of 5 kPa. As shown in Fig. 6, the specific impulses for supercritical cases were greater than 80 % of ideal correct expansion curve value. However, the specific impulses for subcritical cases were less than 80 % of the ideal value. This can be due to the incomplete detonation. For small inner cylinder radius cases (r_i = 0 and 9), the local equivalence ratio is thought to deteriorate in the vicinity of the inner cylinder wall because of the large distance

from the injection position.

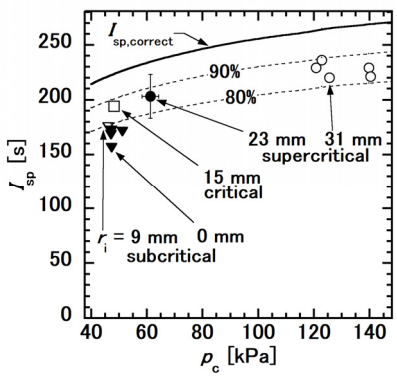

Fig. 6. Dependence of specific impulse on combustion chamber pressure (C_2H_4–O_2, ϕ = 1.18±0.17, $\dot{m}$ = 136±6 g/s, p_b = 5±1 kPa). Symbols are measured data. Error bars are shown only for the case where r_i = 23 mm as a typical example. Solid line is ideal correct expansion curve computed by the NASA CEA code [26].

Figure 7 plots the ratio of I_{sp} to $I_{sp,correct}$ versus the ratio of the height of unburned mixture layer [6] h to the detonation cell width λ. The height of the unburned mixture layer was calculated by $\dot{m}r_{inj}/(\rho A_c D_{CJ})$, here the density was calculated with the ideal gas law at the pressure of the combustion chamber and a temperature of 300 K. The detonation cell width was evaluated approximately using a best fit curve [24] to measured data for stoichiometric ethylene-oxygen mixtures in the Detonation Database [25–28],

$$\lambda = 72.312 p_c^{-1.1362} \tag{2}$$

here λ is in mm and p_c is in kPa. As shown in Fig. 7, for the critical case (r_i = 15 mm) and supercritical case (r_i = 23 and 31 mm), the reduced unburned mixture layer height, h / λ, is relatively large and greater than 6.5. Meanwhile, for the subcritical cases (r_i = 0 and 9 mm), the reduced height is relatively small and less than 4.5. Hence, the critical

condition in the inner cylinder radius (r_i = 15 mm) corresponds to critical condition to the condition in the reduced unburned layer height, i.e., h / λ = 4.5–6.5. These experimental results suggest that the deterioration in the specific impulse can be avoided in the no-inner-cylinder configuration if a sufficient height of the unburned mixture layer is attained by reducing the outer cylinder radius and/or increasing the propellant mass flow rate.

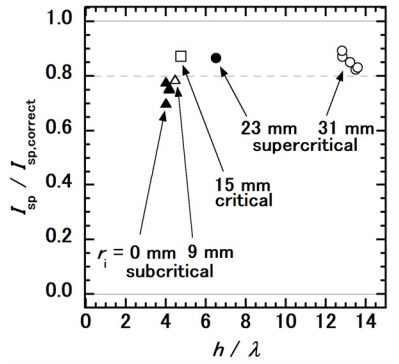

Fig. 7. Dependence of $I_{sp}/I_{sp,orrect}$ on h/λ (C_2H_4–O_2, ϕ = 1.18±0.17, $\dot{m}$ = 136±6 g/s, p_b = 5±1 kPa).

4. Conclusions

We tested a nozzleless RDE with a C_2H_4–O_2 propellant in a low-backpressure environment while varying the inner cylinder radius, r_i, in a range from 0 (no-inner-cylinder configuration) to 31 mm (typical annular configuration). In the experiments, we also performed high-speed imaging of self-luminescence in the combustion chamber and engine plume. In the case of relatively large inner cylinder radii (r_i = 23 and 31 mm), rotating detonation waves in the combustion chamber attached to the inner cylinder surface, whereas for relatively small inner cylinder radii (r_i = 0, 9, and 15 mm), rotating detonation waves were observed to detach from the inner cylinder surface. In these small

inner radii cases, strong chemical luminescence was observed in the plume, probably due to the existence of soot. On the other hand, for cases where r_i = 15, 23, and 31 mm, the specific impulses were greater than 80 % of the ideal value at correct expansion. Meanwhile, for cases r_i = 0 and 9 mm, the specific impulses were below 80 % of the ideal expansion value. This was considered to be due to the imperfect detonation combustion (deflagration combustion) observed in small inner cylinder radius cases. Our results suggest that in our experimental conditions, r_i = 15 mm was close to the critical condition for sustaining rotating detonation in a suitable state for efficient thrust generation.

Acknowledgements

This research was financially supported by the Institute of Space and Astronautical Science (ISAS) / Japan Aerospace Exploration Agency (JAXA), the Nitto Foundation, and the Japanese Society for the Promotion of Science (JSPS) KAKENHI Grant Number 17H03480, 17H06741, and 17K18937.

References

[1] W. Fickett, W.C. Davis, Detonation (1979).

[2] J.H.S. Lee, The Detonation Phenomena (2008).

[3] C.K. Low, Combustion Physics (2006).

[4] K. Kailasanath, AIAA Journal 38 (9) (2000) 1698-1708.

[5] G.D. Roy, S.M. Frolov, A.A. Borisov, D.W. Netzer, Progress Energy Combust. Sci. 30 (6) (2004) 545-672.

[6] F.A. Bykovskii, S.A. Zhdan, E.F. Vedernikov, J. Propul. Power 22 (6) (2006) 1204-1216.

[7] P. Wolański, Proc. Combust. Inst. 34 (1) (2013) 125-158.

[8] F.K. Lu, E.M. Braun, J. Propul. Power 30 (5) (2014) 1125-1142.

[9] H. Nakayama, J. Kasahara, A. Matsuo, I. Funaki, Proc. Combust. Inst. 34 (2013) 1939-1947.

[10] H. Nakayama, T. Moriya, J. Kasahara, A. Matsuo, Y. Sasamoto, I. Funaki, Combust. Flame 159 (2) (2012) 859-869.

[11] Y. Kudo, Y. Nagura, J. Kasahara, Y. Sasamoto, A. Matsuo, Proc. Combust. Inst. 33 (2011) 2319-2326.

[12] Y. Sugiyama, A. Matsuo, H. Nakayama, J. Kasahara, Combust. Sci. Tech. 186 (2014) 1662-1679.

[13] F.A. Bykovskii, S.A. Zhdan, E.F. Vedernikov, Combust. Explosion Shock Waves 47 (2) (2011) 217-225.

[14] S. Nakagami, K. Matsuoka, J. Kasahara, Y. Kumazawa, J. Fujii, A. Matsuo, I. Funaki, J. Propul. Power 33 (1) (2017) 80-88.

[15] S. Nakagami, K. Matsuoka, J. Kasahara, A. Matsuo, I. Funaki, Proc. Combust. Inst. 36 (2017) 2673-2680.

[16] X.M. Tang, J.P. Wang, Y.T. Shao, Combust. Flame 162 (2015) 997-1008.

[17] L. Wei, Z. Jin, L. Shijie, L. Zhiyong, Exp. Therm. Fluid Sci. 62 (2015) 122-130.

[18] V. Anand, A. St. George, E. Gutmark, AIAA Paper 2016-0124 (2016).

[19] H.W. Liepmann, A. roshko, Elements of Gasdynamics

[20] G.P. Sutton, O. Biblarz, Rocket Propulsion Elements, Ninth Ed. (2017).

[21] D.E. Paxson, AIAA Paper 2018-1883 (2018).

[22] J. Kasahara, Y. Kato, K. Ishihara, K. Goto, K. Matsuoka, A. Matsuo, I. Funaki, H. Moriai, D. Nakata, K. Higashino, N Tanatsugu, Application of Detonation Waves to Rocket Engine Chamber, Detonation Control for Propulsion (2018).

[23] NASA-CEA Online, available at <https://www.ipsj.or.jp/journal/submit/ronbun_j_prms.html>

[24] Y. Nagura, J. Kasahara, A. Matsuo, Shock Waves 26(5) (2016) 645–656.

[25] S. Abid, G. Dupre, C. Paillard, Prog. Astronaut. Aeronaut. 153 (1991) 162–181.

[26] R. Knystautas, J.H.S. Lee, C. Guirao, Combust. Flame 48 (1982) 63–83.

[27] R.A. Strehlow, AIAA J. 7 (3) (1969) 492–496.

[28] M. Kaneshige, J.E. Shepherd, Technical Report FM97-8, GALCIT (1997).

Supplemental Material (Movie Caption)

Movie S2(a): Axial movie of self-luminescence in the combustion chamber taken with a high-speed camera (ri = 0 mm) (.mov file).

Movie S2(b): Axial movie of self-luminescence in the combustion chamber taken with a high-speed camera (ri = 9 mm) (.mov file).

Movie S2 (c): Axial movie of self-luminescence in the combustion chamber taken with a high-speed camera ri

= 15 mm) (.mov file).

Movie S2 (d): Axial movie of self-luminescence in the combustion chamber taken with a high-speed camera *r*i = 23 mm) (.mov file).

Movie S2 (e): Axial movie of self-luminescence in the combustion chamber taken with a high-speed camera *r*i = 31 mm) (.mov file).

Movie S3 (a): Lateral movie of self-luminescence in the combustion chamber taken with the high-speed camera *r*i = 0 mm) (.mov file).

Movie S3 (b): Lateral movie of self-luminescence in the combustion chamber taken with a high-speed camera *r*i = 9 mm) (.mov file).

Movie S3 (c): Lateral movie of self-luminescence in the combustion chamber taken with a high-speed camera *r*i=15 mm) (.mov file).

Movie S3 (d): Lateral movie of self-luminescence in the combustion chamber taken with a high-speed camera *r*i = 23 mm) (.mov file).

Movie S3 (e): Lateral movie of self-luminescence in the combustion chamber taken with a high-speed camera *r*i = 31 mm) (.mov file)